Science of the Total Environment 650 (2019) 1805–1817

Contents lists available at ScienceDirect

Science of the Total Environment

journal homepage: www.elsevier.com/locate/scitotenv

The exposure of slums to high temperature: Morphology-based local scale thermal patterns

Jiong Wang *, Monika Kuffer, Richard Sliuzas, Divyani Kohli

Faculty of Geo-Information Science and Earth Observation (ITC), University of Twente, P.O. Box 217, 7500 AE Enschede, the Netherlands

HIGHLIGHTS

- A workflow of investigating local scale temperature patterns is proposed.
- Morphological parameters characterize the intrinsic temperature patterns without the restriction of the pixel size.
- In particular, slums are exposed to locally high temperature.
- Larger slums tend to be exposed to more intense locally high temperature.

GRAPHIC ABSTRACT

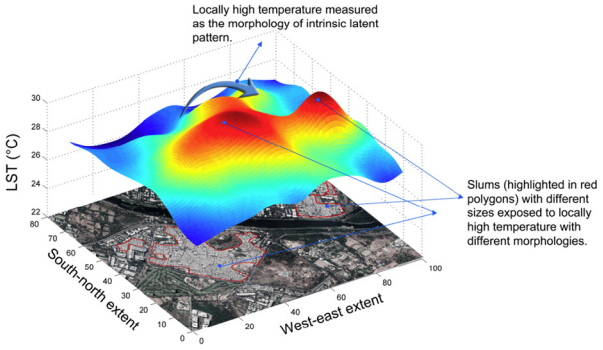

ARTICLE INFO

Article history:
Received 25 May 2018
Received in revised form 23 September 2018
Accepted 25 September 2018
Available online 26 September 2018

Editor: SCOTT SHERIDAN

Keywords:
Slums
Local scale
LST
Morphological patterns
MODIS
Ahmedabad
India

ABSTRACT

Heat exposure has become a global threat to human health and life with increasing temperatures and frequency of extreme heat events. Considering risk as a function of both heat vulnerability and hazard intensity, this study examines whether poor urban dwellers residing in slums are exposed to higher temperature, adding to their vulnerable demographic and health conditions. Instead of being restricted by sampling size of pixels or other land surface zones, this study follows the intrinsic latent patterns of the heat phenomenon to examine the association between small clusters of slums and heat patterns. Remotely sensed land surface temperature (LST) datasets of moderate resolution are employed to derive the morphological features of the temperature patterns in the city of Ahmedabad, India at the local scale. The optimal representations of temperature pattern morphology are learnt automatically from temporally adjacent images without manually choosing model hyper-parameters. The morphological features are then evaluated to identify the local scale temperature pattern at slum locations. Results show that in particular locations with slums are exposed to a locally high temperature. More specifically, larger slums tend to be exposed to a more intense locally high temperature compared to smaller slums. Due to the small size of slums in Ahmedabad, it is hard to conclude whether slums are impacting the locally high temperature, or slums are more likely to be located in poorly built places already with a locally high temperature. This study complements the missing dimension of hazard investigation to heat-related risk analysis of slums. The study developed a workflow of exploring the temperature patterns at the local scale and examination of heat exposure of slums. It extends the conventional city scale urban temperature analysis into local scales and introduces morphological measurements as new parameters to quantify temperature patterns at a more detailed level.

* Corresponding author.
E-mail addresses: j.wang-4@utwente.nl (J. Wang), m.kuffer@utwente.nl (M. Kuffer), r.sliuzas@utwente.nl (R. Sliuzas), d.kohli@utwente.nl (D. Kohli).

https://doi.org/10.1016/j.scitotenv.2018.09.324
0048-9697/

1. Introduction

1.1. Excessive heat and extreme heat events

The global temperature keeps rising (Change, 2014) along with disproportionate variations leading to a change in the frequency of extreme climate events and causing the majority of the global land surface to experience an increase of extreme heat events (Stocker, 2014; Wigley, 2009). Even worse, as near-surface temperature is largely governed by the land surface specification, the built environment with more dense buildings, impervious surfaces, and less vegetation within urban areas exhibits a doubled warming rate of the global level (Stone et al., 2013). Such higher temperatures in urban areas, known as Urban Heat Islands (UHI) (Balchin and Pye, 1947), have been detected and documented for nearly 200 years (Howard, 1818, 1833). Their magnitude could be up to 12 °C in clear and calm weather condition (Landsberg, 1981; Oke, 1973, 1981; Oke, 1982). With the advancement of airborne sensors in monitoring land surface temperature (LST), the surface UHI is also considered as an important indicator of urban environment (Rao, 1972; Roth et al., 1989; Streutker, 2002, 2003; Voogt and Oke, 1997).

1.2. Discrepancies in local scale heat related risk analysis

With increasingly high temperatures in urban areas, a paradigm shift has can be observed from disaster response management to proactive risk management (Assembly, 2015; Change, 2014; Chu, 2015; Leal Filho, 2016). Due to the intra-urban heat risk variations within cities especially in developing countries, urban dwellers are more likely to be affected by heat-related morbidity and mortality risks (Kjellstrom et al., 2007; McGeehin and Mirabelli, 2001; Romero-Lankao et al., 2016). Thus feasible and effective risk management is recommended to be local level oriented and prioritized for groups with the highest heat risk (Baker, 2012; Chang et al., 2007; Chu, 2015; Larsen, 2015). Only a limited number of studies in South Asian cities such as Mumbai, Delhi, Ahmedabad and Surat in India localized the heat related risks by suggesting that slum dwellers are more vulnerable than others to extreme heat due to poor demographic, physiological and economic conditions (Hajat et al., 2005; Nag et al., 2009; Rathi et al., 2017; Romero-Lankao et al., 2016; Tran et al., 2013). These studies only addressed risks by exclusively focusing on the heat vulnerability in terms of socioeconomic attributes (Chaudhury et al., 2000; Dash and Kjellstrom, 2011). However, as risk is a function of hazard intensity and vulnerability of people exposed to the hazard (Blaikie et al., 2014; Brooks et al., 2005). Only one related study in Ahmedabad suggested that slum dwellers may experience a higher temperature by using a ground survey covering only a limited number of households (Knowlton et al., 2014). The local scale exposure pattern of vulnerable slum dwellers to high-temperature hazards in a whole city has never been examined.

It has been widely acknowledged that local scale temperature variations within urban areas should not be neglected due to the diverse intra-urban land surface specifications (Arnfield, 2003; Kalnay and Cai, 2003). Slums defined as areas lacking access to satisfactory water, sanitation, durable housing or tenure security (Un-Habitat, 2016), are with dense and poorly built forms and materials subject to extreme heat. Unfortunately, high temperature patterns such as the UHI phenomenon depicted either through *in-situ* measurements or satellite images are dominated by the "urban-rural" dichotomy, providing aggregated information at city or regional scales (Stewart, 2011a; Stewart, 2011b; Stewart and Oke, 2012). A handful attempts using thermal satellite images in examination of the local scale temperature variations are either restricted by the pixel level or averaging the pixel values into census tracts or districts bounded by road networks (Amiri et al., 2009; Buyantuyev and Wu, 2010; Chang et al., 2007; Connors et al., 2013; Coutts et al., 2016; Kroeger et al., 2018; Norton et al., 2015; Preston et al., 2011; Stewart and Oke, 2009; Svensson and Eliasson, 2002; Yin et al., 2018). These studies essentially focused on temperature values with different granularity instead of the intrinsic temperature patterns. One exception, focusing on local scale LST variation at the phenomenon level, is based upon visual identification of surface heat islands (Gulbe et al., 2017).

1.3. The temperature patterns of slum areas

Temperature patterns are essentially continuous in space and time hidden in noisy discrete observations in the form of *in-situ* measurements or satellite images, which should be recovered through modeling (Goodchild, 1987). The UHI at city or regional scale provides an inspiring concept for characterizing temperature patterns through spatial or morphological parameters such as extent, magnitude and location, and shows an association between these parameters and city size and location (Quan et al., 2014; Streutker, 2002, 2003). These morphological parameters capture the intrinsic patterns of the temperature phenomenon instead of being restricted by the pixel size or artificially defined land patch units. Recognizing such benefits, this study builds on the strength of morphological parameters to characterize the local scale temperature patterns. Similar to the city or regional scale UHI, the presence of slums are to be associated with local scale morphological features of temperature patterns such as "island-shaped" temperature bumps. Therefore, this study aims to answer: (1) whether slums are experiencing higher temperature compared to other built environments, and (2) how slums are associated with local scale temperature patterns?

2. Study area and data

2.1. Study area

The case study city of Ahmedabad, India is the sixth largest city of India with a population of approximately 5.6 million and less than 5% of the population lives in slums according to the census (Chandramouli and General, 2011). However, this statistic excludes a large part of physically deprived areas such as chawls that are working class housing of very poor conditions. Local data from the municipality conclude a much larger amount of population (around 18%) living in slum conditions, which also matches with insights we have from field visits (therefore this data is used as a reference in this study) (Garland, 2016). In general, such areas suffer from high temperature and frequent heat waves (Azhar et al., 2014). The average summer temperature is 38.8 °C through March to June. The heat waves can intensify the daily maxima during the hottest month of May, for instance, the worst heat wave in the recent history of Ahmedabad (in 2010) increased the temperature up to 46.8 °C (Knowlton et al., 2014).

The 56 × 44 km rectangular shaped study area encompasses the entire Ahmedabad municipality and its rural surroundings to represent land use and land cover diversity (Fig. 1). The coordinates of the northwestern and southeastern corners are "23.22 N, 72.31E" and "22.83 N, 72.84E", respectively. The municipal boundary along with the administrative wards is highlighted by black solid lines.

2.2. Data

Using dense automatic weather station (AWS) networks to observe near-surface air temperature is not possible in developing countries, where commonly only one AWS (distant from urban areas) can be found at the airport. Alternatively, the LST recorded by thermal satellite images with resolutions coarser than 250 m can be used as a strong indicator of the variation of near surface air temperature despite of distinctively different meteorological and thermodynamic processes between near surface air temperature and the LST (Coutts et al., 2016; Klok et al., 2012; Stoll and Brazel, 1992).

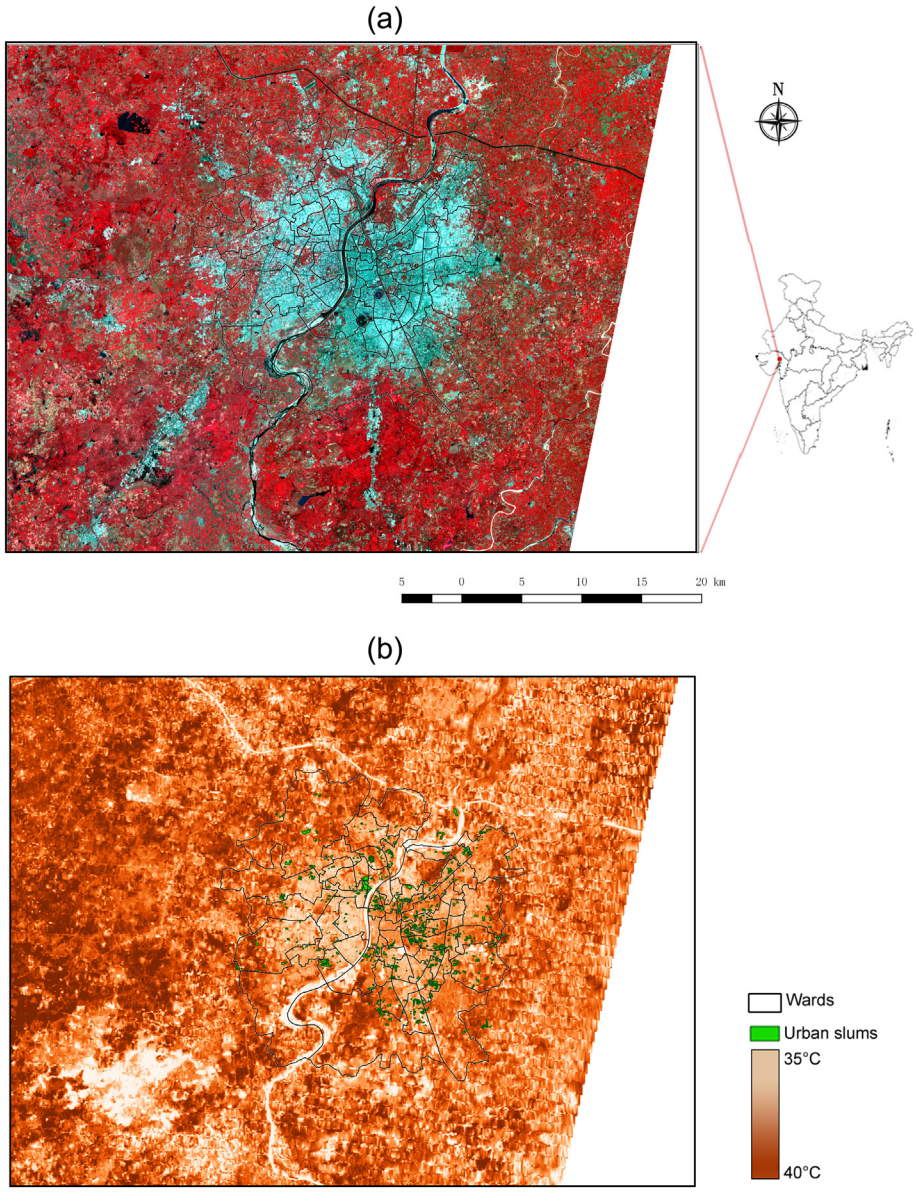

Fig. 1. The study area of Ahmedabad, India shown as (a) false-color Landsat 7 ETM+ image highlighting the built-up environment of the urban core and rural surroundings, and (b) the Landsat 7 ETM+ thermal image acquired on May 02, 2010 with urban slums shown as green polygons.

Considering that Ahmedabad experiences the highest temperature in May, the MODerate-resolution Imaging Spectroradiometer (MODIS) Terra (MOD11A2) and Aqua (MYD11A2) V6 LST/E 8-Day L3 Global 1 km Grid products (https://ladsweb.modaps.eosdis.nasa.gov/search/) are used to capture the average LST patterns every 8 days in May 2010 corresponding to the year of slum data acquirement. At local time, Terra captures the LST at 10:30 and 22:30, while Aqua captures the LST at 01:30 and 13:30. Generated by the split-window LST algorithm (Wan and Dozier, 1996), these daily products are validated with an accuracy better than 1 °C (0.5 °C in most cases) (Wan, 2008, 2014). Four sets of 8-day average daily LST images spanning through the entire month of May are used providing average daily LST patterns of 1st ~ 8th, 9th ~ 16th, 17th ~ 24th, and 25th ~ 31st, May, respectively. Each set contains the Terra and Aqua images at the four time points, thus 16 images are used in total. The urban slum boundaries are obtained from the municipality of Ahmedabad, India, 2010 (Fig. 1 (b)).

3. Methodology

Following the concept of the UHI at the city or regional scale, the latent patterns of the LST is recovered from the noisy observation for morphological characterization of slums locations to examine whether "island-shaped" morphological features can be associated with the presence of slums.

3.1. Latent patterns of temperature variations

Remotely sensed LST suffers from noise and missing data due to undesirable weather conditions, atmospheric and radiation interferences, or sensor malfunctioning (Li et al., 2013). To overcome these limitations, one can assume the LST of coarse resolution to be a satisfactory proxy of the variation of near surface air temperature (Coutts et al., 2016), which is a continuous latent process hidden in discrete noisy image data, which needs to be recovered (Wang et al., 2015b). The benefit of the recovery is twofold: (1) the missing values are filled and noises are

smoothen, and (2) the latent continuous process supports efficient pattern analysis (Goodchild, 1987). While previous studies have shown the strength of parametric and non-parametric models in recovering of the latent LST (Rajasekar and Weng, 2009; Streutker, 2002), the prior assumption of forms and hyper-parameters (kernel size) required are artificially selected, leading to rigorous representation of the latent LST process at the city scale. Thus the variations within cities are ignored.

The Multi-Task Gaussian Process (MTGP) model is applied in this study to recover the latent temperature patterns as the model takes advantage of both the flexibility of non-parametric modeling and machine learning (Bonilla et al., 2008; Wang et al., 2015b). The MTGP model is an extension of the Gaussian Process (GP) (Rasmussen, 2006) model (known as Kriging approach in geographic science) by assuming multiple GPs are correlated, where the multiple processes are called Multi-Task GPs. When this is applied to LST datasets, the MTGP model not only treats temperature variations in one image to be spatially correlated but also considers temporally adjacent images to be correlated as Multi-Tasks. Thus the continuous latent patterns of the LST in one image can be recovered from the observations in that image and from temporally adjacent images. In this study, the daytime LST images acquired at 10:30 and 13:30 on the same day (within 3 h) with similar spatial variation patterns are considered as two correlated processes or tasks in the MTGP model despite of their difference in absolute temperature value. Same assumption applies to the two nighttime images acquired at 22:30 and 1:30. The MTGP automatically selects the optimal hyper-parameters to properly resemble the variation of the temperature while smoothing out noises. The robustness of the MTGP in recovering latent LST patterns by using images with extensive missing pixels has been well documented (Wang et al., 2015b) and details can be found in the Appendix A.

3.2. The morphology of latent LST patterns at local scale

The spatial analysis is subject to the issue of scale (Woodcock and Strahler, 1987), which defines a rough range of the analysis (Arnfield, 2003; Stewart and Oke, 2012). For example, "city-scale" varies along with the size of cities. The situation also applies to local scale analysis of LST patterns as the latent LST patterns can be contiguous, crossed or overlapped to form morphological features with different sizes. As shown in Fig. 2, it can be difficult to decide whether the ridge or cap shaped latent patterns labeled "1" and "3" (highlighted by the solid red line) are close enough to each other. They can be treated either as separated or as single "island-shaped" morphological feature highlighted by the green dashed line ignoring the rut or cup shaped pattern labeled "2".

The Multi-Scale Shape Index (MSSI) (Bonde et al., 2013) as an extension of Koenderink's Shape Index (SI) (Koenderink and van Doorn, 1992) is applied to evaluate the morphological features of the latent LST patterns at the optimal scale. The evaluation thus contains two steps: 1) optimal scale selection in the scale space (Lowe, 1999), and 2) the morphological evaluation.

The scale space S is generated by projecting the latent LST patterns $f(s)$ through

$$S(f(s),\theta) = f(s) * k(s-u,\theta) = \int_0^s f(u)k(s-u,\theta)du, \tag{1}$$

where $k(\cdot,\cdot)$ is the Gaussian kernel with varying smoothing magnitude θ centered at each location u on the surface s. Thus S is a 3-dimensional space, where different scales of the original 2-dimensional LST patterns produced by the smoothing kernel are distributed along the third dimension.

Selecting the optimal scale at each pixel location implies to find the characteristic scale that best manifests the local feature at that location. The local feature should be most stable along the change of the kernel smoothing magnitude θ at the characteristic scale. Thus the optimal scale minimizes the traveled distance of the original pixel shifted by the smoothing kernel. While the distance shifted on an image surface is the difference between original and smoothed pixel values, the optimal scale θ^* can be found as

$$\frac{\partial d}{\partial \theta} = \frac{\partial\left(\|S(f,\theta)-f\|^2\right)}{\partial\theta} = 0. \tag{2}$$

where the zero derivative means that the local feature at the optimal scale should remain stable as the scale changes.

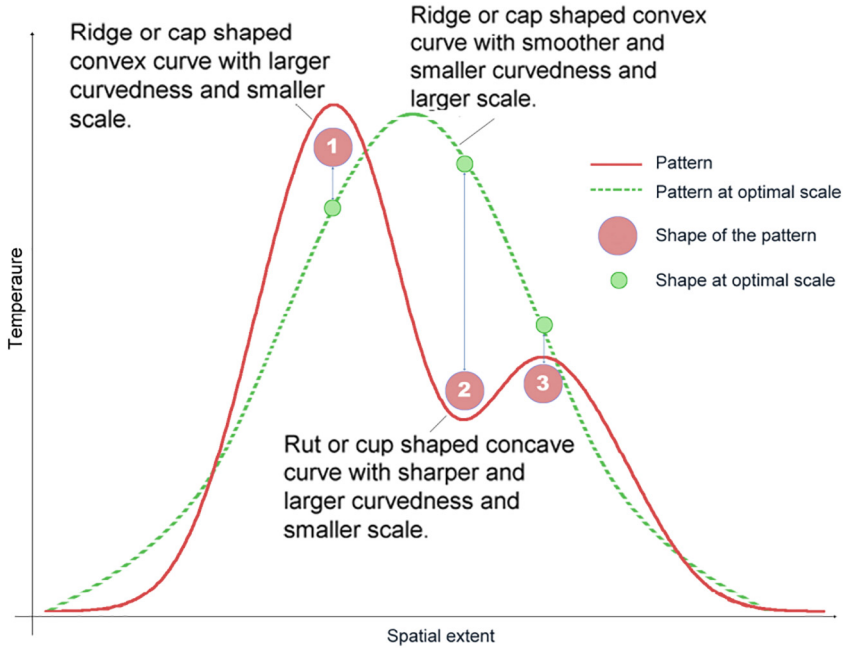

Fig. 2. One dimensional schematic illustration of how local temperature variations should be evaluated at proper scale.

Then the SI is evaluated at the optimal scale at each pixel location on a surface to obtain the MSSI. The SI is *defined as*

$$SI = \frac{2}{\pi}\arctan\frac{\kappa_2+\kappa_1}{\kappa_2-\kappa_1}, SI\in[-1,1], \quad (3)$$

where κ_1 and κ_2 ($\kappa_1 \geq \kappa_2$) are the principle curvatures, which can be evaluated through eigenvalues of the Hessian matrix. The SI encodes the morphological transition among typical features such as cup, rut, saddle, ridge, and cap within the interval $[-1, 1]$. Thus it captures the spatial and magnitude properties of local LST patterns.

Along with the MSSI, the curvedness, which is inverse proportional to the optimal size or scale, is also used to distinguish morphological features with the same shape but different sizes. At the optimal scale θ^*, the curvedness is obtained based upon principle curvatures as

$$curvedness = \sqrt{\frac{\kappa_1^2+\kappa_2^2}{2}}. \quad (7)$$

A complete profile of latent LST patterns can be described with the combination of the MSSI, curvedness or optimal scale.

4. Results

4.1. The recovery of latent LST patterns

The MODIS LST image data of the study area acquired at 01:30 on May 01, 2010 is used to illustrate the reliability of the latent LST pattern recovery. A rarely found original image (Fig. 4(a)) without missing pixel values is artificially degraded by randomly deleting 10% of the total pixels to model cloud contaminated images (Fig. 4(b)). The recovered latent LST is shown in Fig. 4(c). By maximizing the marginal likelihood in Eq. (6), the recovered latent LST avoids either under- or over-fitting. The recovery fills the missing values and popularizes the resolution of the image by a factor of 2 so that the continuous latent LST is smooth enough for pattern analysis. The recovery has been repeated 30 times to ensure robustness. The average of the 30-time-repetition shows the difference between the observed and recovered latent LST to be acceptable with RMSE of 0.086 °C (Fig. 4(d)). The statistical summary of the observed and recovered LST is presented in Table 1, which indicates the validity of the assumption applied in the MTGP model.

Relying on the robustness of the MTGP modeling, the latent diurnal LST patterns in May are recovered by using the MODIS/Terra (MOD11A2) and MODIS/Aqua (MYD11A2) V6 LST/E 8-Day L3 Global 1 km Grid products. The 8-Day composite data can capture well the average regulations of diurnal LST patterns in May. The 8-day average latent diurnal LST patterns through 1st to 8th of May 2010 are recovered and visualized in Fig. 5. The average LST increases from 26.79 °C at 01:30 to 43.75 °C at 10:30, and reaches the daily maximum of 49.17 °C at 13:30, then drops to 28.71 °C at 22:30.

Different legend intervals are applied for the LST patterns in Fig. 5 to highlight the spatial distribution of high and low temperature within the same image. During the day, the highest LST values are found in rural areas to the west of the study area, which are mostly covered by seasonal agricultural land, which is not irrigated. Once the solar radiation is available, the input energy is released as sensible heat leading to higher temperature than found at places with moisture available for evapotranspiration. During the night, high LST around the urban core is more prominent due to its high heat capacity with delayed a rise of temperature. Thus the LST of the entire study area drops down after the sunset, the slower decrease of the LST within the urban core area results into higher LST compared to rural areas. Such diurnal LST regulations are well documented in previous surface UHI (SUHI) studies (Göttsche and Olesen, 2001; Imhoff et al., 2010). Areas with lower LST are found both to the southern and eastern part of the study area being occupied by fully irrigated croplands, where enough water in the soil is available for evapotranspiration and split the input energy of solar radiation more into latent heat and less into sensible heat.

Table 1
Comparison between observed original LST and recovered LST patterns (°C).

	Min	Max	Mean	Median	Std.
Observed	11.05	17.45	13.13	12.81	1.10
Latent	11.43	17.40	13.14	12.83	1.09

4.2. The morphology of latent LST patterns

Given the diurnal patterns of the LST shown in Section 4.1, the nighttime LST patterns (Fig. 5(a) and (d)), which exhibits full response of the urban area to the solar radiation, is more meaningful to study how citizens especially slum dwellers are exposed to a potential high temperature. If only the daytime snapshots of the LST dynamics are used, the association of the patterns between the LST and slums can be substantially underestimated. Thus the following investigations focus on nighttime LST patterns.

As interpreted in Section 3.2, the MSSI measures morphological features such as cup, rut, saddle, ridge, and cap at the optimal local scale. Take the latent LST patterns in Fig. 4(c) acquired at 01:30 on May 1st as an example, a visually random distribution of morphological features can be observed in Fig. 6(a). This is due to the Shape Index (SI) (Eq. (3)) is measured uniformly at pixel level without considering the scale. Thus the patterns belonging to the same morphological feature are unnecessarily evaluated individually. In contrast, the MSSI can better capture the morphological features by showing meaningful distributions (Fig. 6(b)). For instance, the visually detectable cap shaped morphologies in urban areas (highlighted by the black boundary) in Fig. 4(c) are properly evaluated as larger features where most of the pixels are estimated as positive MSSI. The cup shaped feature to the northeast of the study area is also a satisfying example as a cluster of negative MSSIs. Whereas the variations inside this large cup shaped features are improperly captured by applying the SI at pixel level, producing a fragmented morphological evaluation (Fig. 6(a)).

4.3. The local scale thermal patterns of urban slums

The MSSI not only delineates the spatial morphology of how the temperature at a location is different from its surroundings but also encodes the extent of the difference. As shown in Fig. 3, a location with a MSSI greater than 0.5 means that the temperature at this location is higher than the surroundings, while a MSSI of 0–0.5 means the temperature at this location is only higher than part of its surroundings. Furthermore, the curvedness measures the magnitude of the locally high or low LST. For example, large curvedness indicates large LST gradient and sharp contrast leading to a prominent morphological feature.

To examine whether slums are exposed to a locally high temperature, we need to check whether the location with the presence of slums is associated with a positive MSSI. For illustration, a 1-dimensional sample is drawn from the central cross-section of the study area to evaluate the association between the local scale LST pattern at 01:30 on May 1st and the distribution pattern of slums (Fig. 7(a)). The 1-dimensional LST pattern and slum distribution are shown in Fig. 7(b) and (c), respectively. The slums are concentrated in urban areas with no values at both ends of the 1-dimensional sample. The corresponding MSSI and curvedness of the sample LST are shown in Fig. 7(d) and (e), respectively. The scale inversely proportional to the curvedness is indicated in color (Fig. 9(e)). The presence of slums roughly corresponds to locally higher LST shown as yellow bars (Fig. 7(b) and (c)). These places are all associated with positive MSSI values (Fig. 7(d)). The highest LST shown by the yellow bars to the right are evaluated with a MSSI of nearly 1 (Fig. 7(d)) indicating a cap shaped morphology not observable in the 1-dimensional illustration. This cap

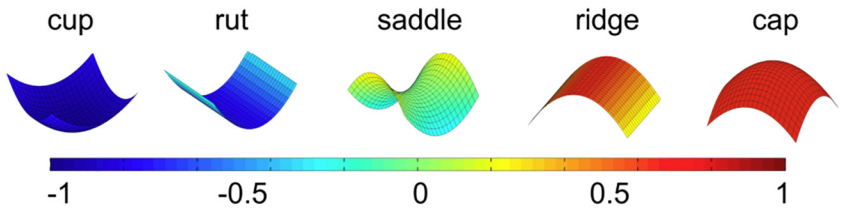

Fig. 3. The surface morphology in the range of the Shape Index (SI).

shaped LST morphology covers a large area and thus is evaluated with low curvedness and high value of scale (Fig. 7(e)). Fewer slums are found to the west of the urban area (highlighted by the yellow bars to the left). These slums are also associated with positive MSSI values with sharp curvedness and small scale LST morphology (Fig. 7(d) and (e)).

To further investigate the association between the local scale LST morphology and the presence of slums, scatter plots (Fig. 8) of the slum coverage fraction and the LST morphology at each of 500 × 500 m grid are shown in Fig. 4. Considering the small size of slums relative to the grid size, the morphological feature evaluated at each pixel location is ensured to cover the slums in the pixel. Thus slums can be treated as fully exposed to the morphological feature. Fig. 8(a) not only confirms the findings of Fig. 7 showing the presence of slums is associated with positive MSSI, but also showing a positive correlation between the slum coverage fraction and the MSSI. This means that larger slums are more likely to be located at places with a locally higher temperature. In addition, the slum coverage fraction is negatively correlated with the curvedness meaning that the temperature difference at the locations of larger slums can be more preeminent than those at the locations of smaller slums (Fig. 8(b)). However, the correlations shown in both Fig. 8(a) and (b) weaken as the slum coverage fraction exceeds 15%.

4.4. Comparison of LST patterns of urban slums

Given the exposure of slums to locally high temperature, the correlations shown in Fig. 8 make it intriguing to examine how temperature patterns differ between slum and non-slum locations. This can be achieved through comparing the LST patterns of different land use types with and without the presence of slums. For this purpose, the major land use and land cover within the study area are extracted based upon the primary and secondary classes of the Anderson classification system (Anderson, 1976) including residential (predominantly with living apartments), commercial (predominantly for sale of products and services), mixed-use (residential, commercial and other built

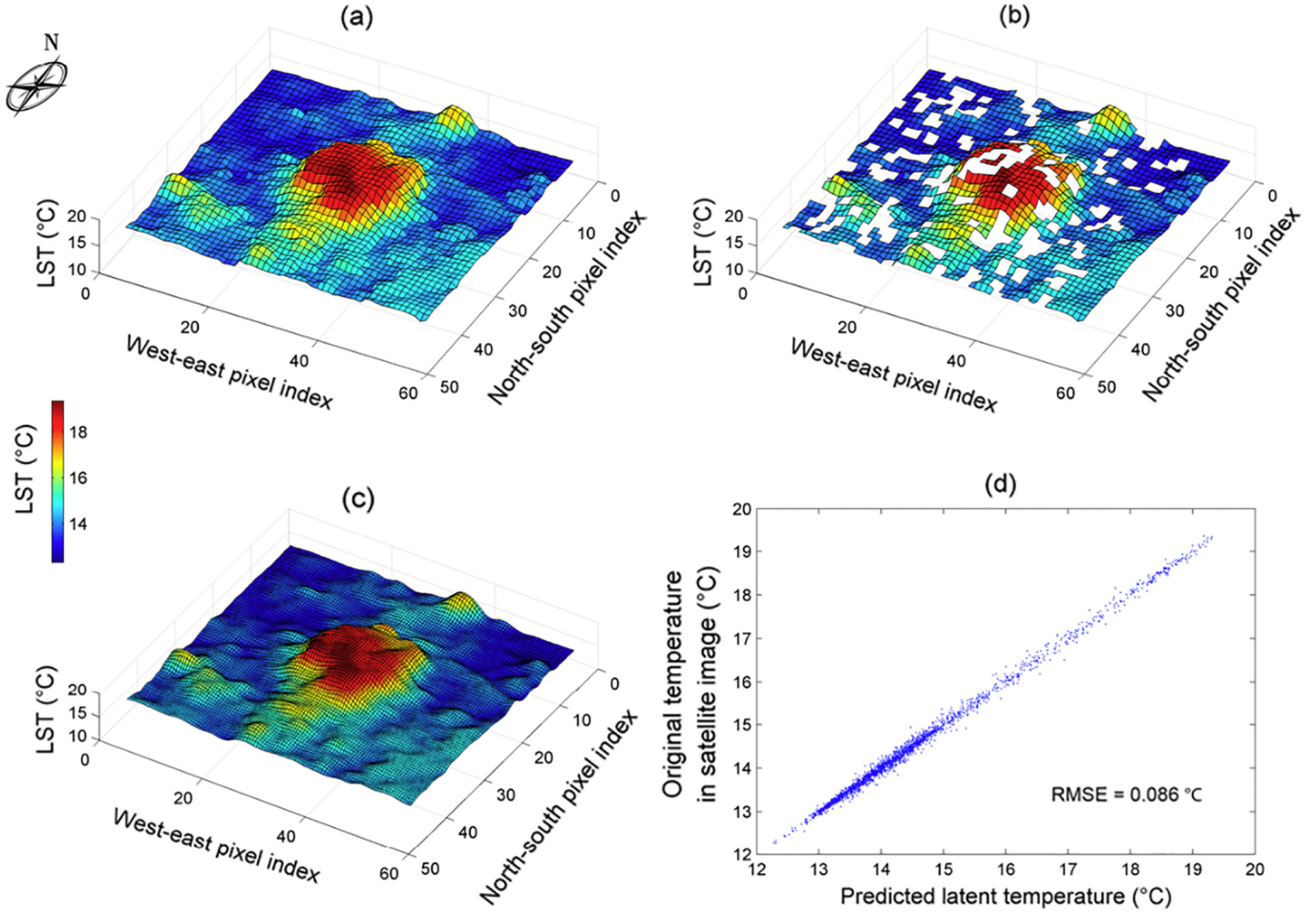

Fig. 4. The Gaussian Process using machine learning mechanism for recovering temperature patterns. (a) original LST image acquired at 01:30 on May 01, 2010, (b) LST image with 15% artificially deleted pixels, (c) latent LST patterns recovered from the artificially manipulated image, and (d) comparison between original and recovered LST datasets.

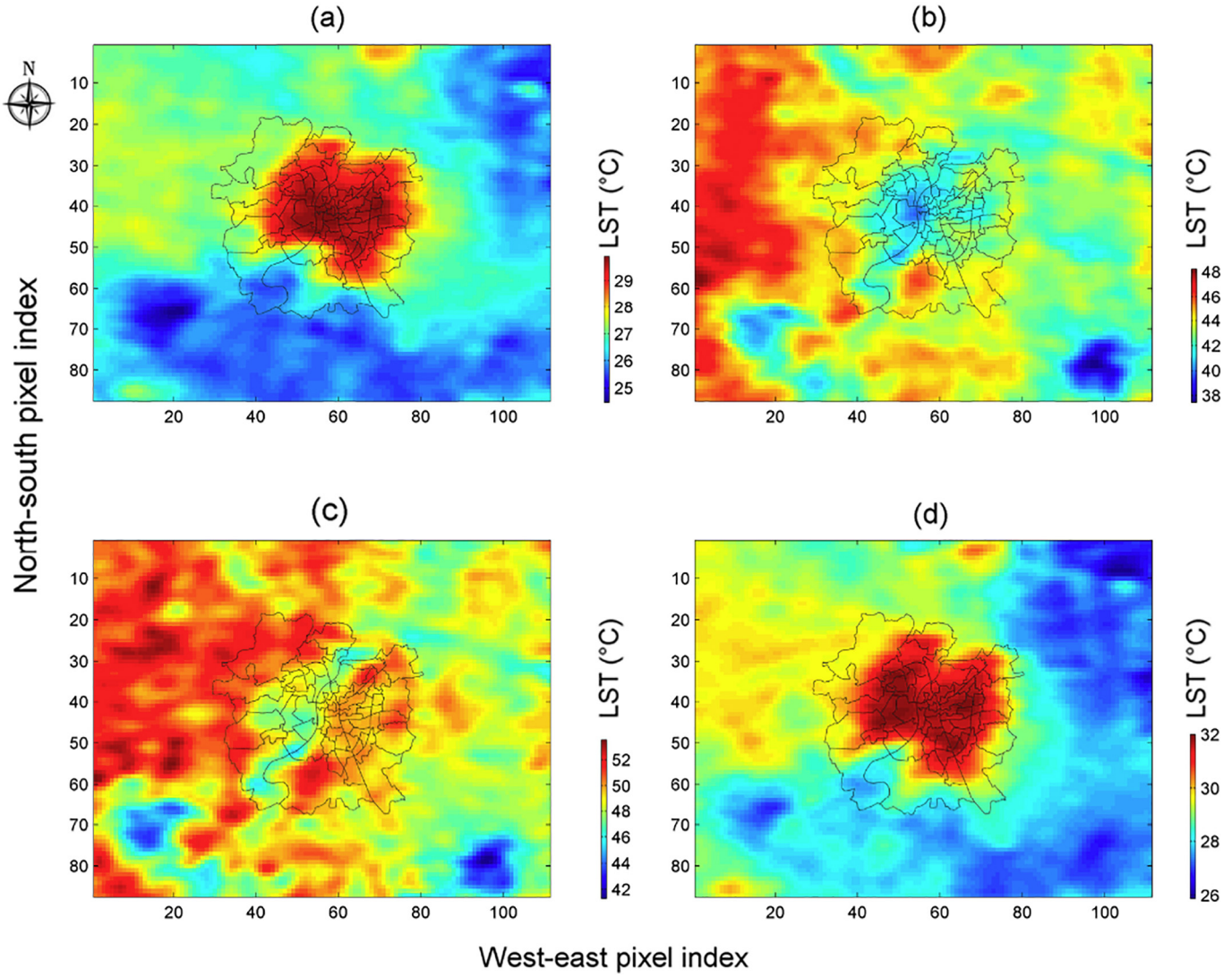

Fig. 5. The 8-day average daily LST patterns at (a) 01:30, (b) 10:30, (c) 13:30, and (d) 22:30 of May 1–8, 2010.

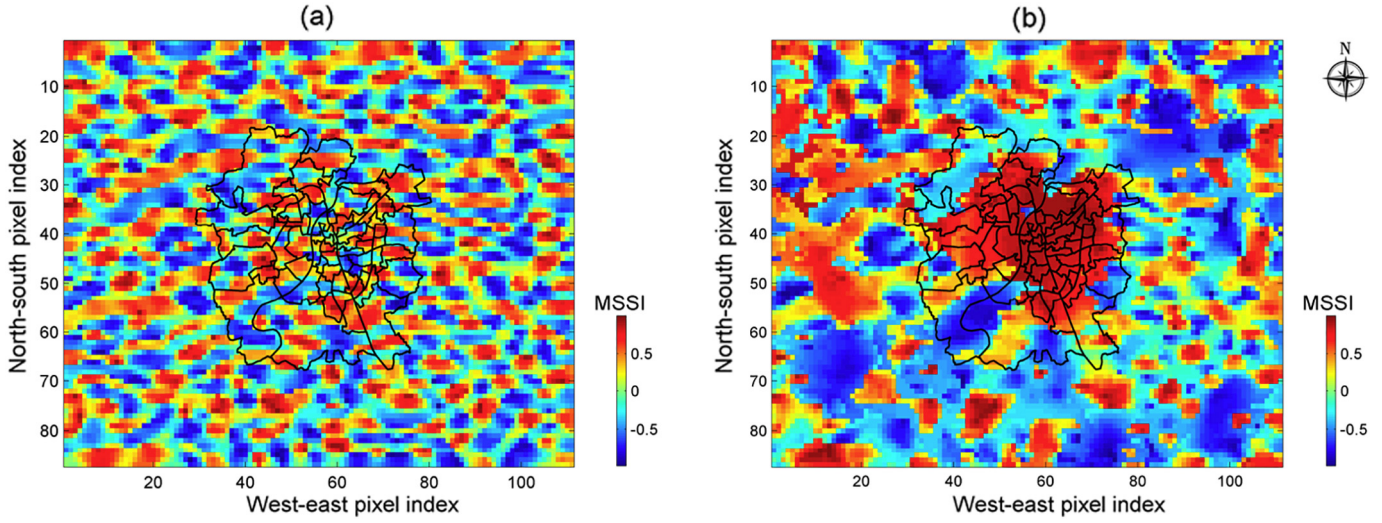

Fig. 6. The morphology of latent LST at 01:30 on May 01, 2010. (a) The SI directly applied to the LST patterns without considering the scales of morphological features. (b) The multi-scale SI evaluated at each pixel location at its optimal scale.

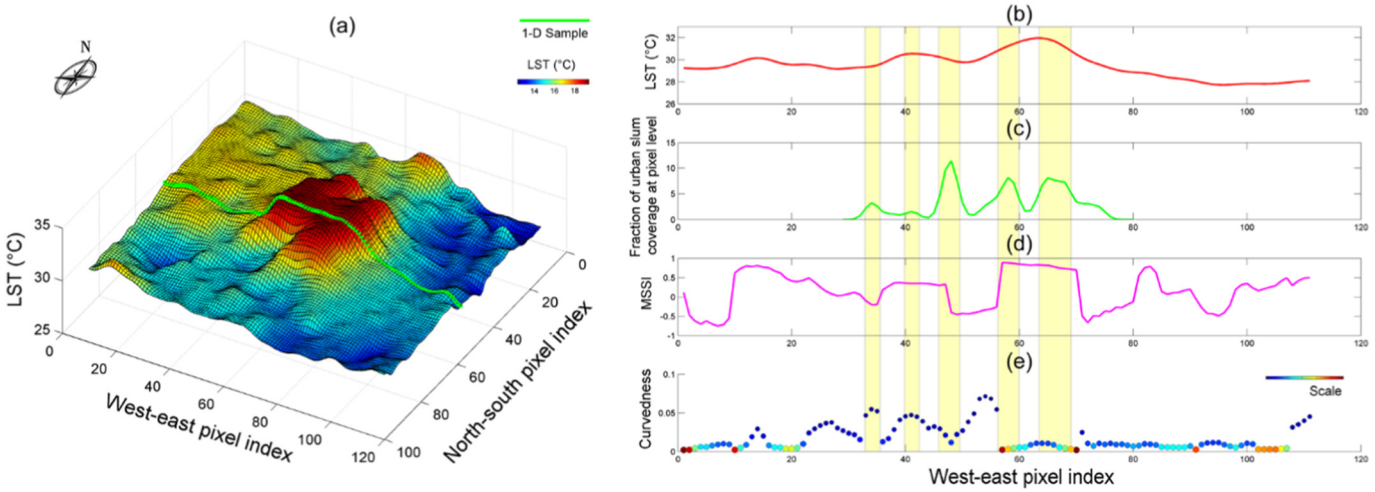

Fig. 7. One dimensional details of the evaluation of SI, curvedness, and scale/size. (a) One dimensional sample selection, (b) sample shown in one dimension, (c) corresponding slum fraction coverage in one dimension, (d) the corresponding multi-scale SI and (e) curvedness and scale/size (locally higher LST as shows as yellow bars).

environment could not be mapped individually), industrial (light and heavy manufacturing plants), and agricultural lands (primarily for production of food and fiber). The seasonal agricultural land is excluded from the analysis because it is located beyond the urban area. Waterbodies (both natural and artificial rivers and lakes) are included as water within the urban core area being an important factor in governing the local scale climate. All pixels containing slums are considered as one class.

The median value of LST for each land use and cover type is shown in Fig. 9. Although the highest LST is found in residential areas, the median LST at the residential areas is 29.59 °C and lower than 31.27 °C found at places with presence of slums. Furthermore, 50% of the LST values are found at the high end of the plot of places with slums. High median LSTs are also found for commercial and industrial land uses with values of 30.89 °C and 30.61 °C. These areas are often densely built and industrial plants may not only absorb solar radiation but also emit anthropogenic heats. The LST of non-seasonal agricultural has the widest LST range, which may be due to irrigation and presence of waterbodies. Static waterbodies may absorb energy during the day and become warm, whereas flowing water of the Sabarmati River can be much cooler. A similar situation is found in MSSI (Fig. 9(b)), where values of places with slums are clustered at the higher end with a maximum value of 0.98. Only the lower quartile (25%) of the MSSI values are below 0.6 meaning that the morphology of the LST patterns around slums are nearly cap shaped. Commercial, industrial and mixed-use lands also tend to contribute to locally high LST. Waterbodies can be positive because the high specific heat capacity of water, which can lead to locally higher LST during the nighttime. The lower three quartiles of the curvedness of the LST morphology at places with slums (comprising 75% of the values) are concentrated at the lower end with a median of 0.01. This means that these places are more likely to intensify the prominence of locally high temperature.

Combining the findings of Section 4.3, one can conclude that slums are likely to be located at places with higher temperature. However, due to the small size of slums within a pixel, it is difficult to quantitatively identify the major factors contributing to the locally high LST at this point.

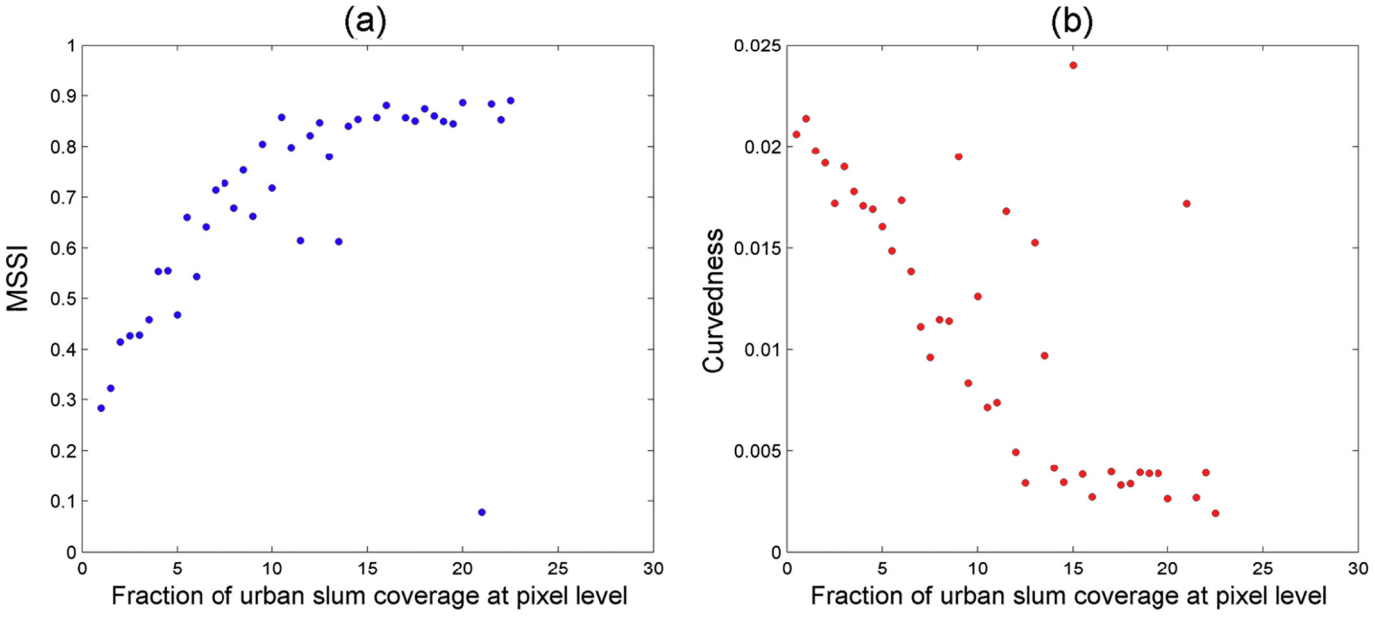

Fig. 8. The association between urban slum fraction coverage and morphology of the latent LST patterns represented as (a) the MSSI and (b) curvedness.

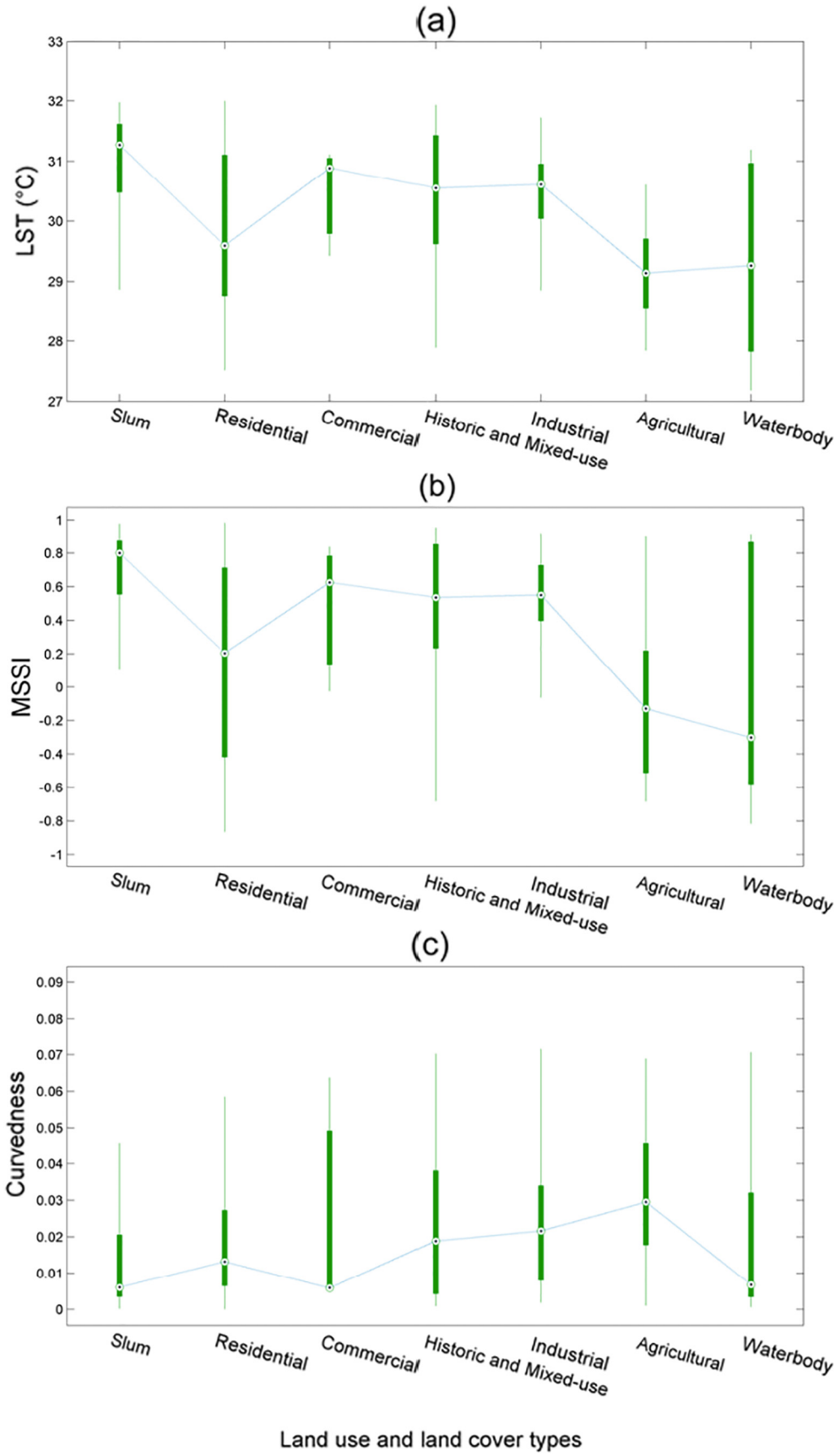

Fig. 9. The LST patterns over different land use and land cover types shown as statistical distributions of (a) the LST, (b) the MSSI, and (c) the curvedness through boxplots.

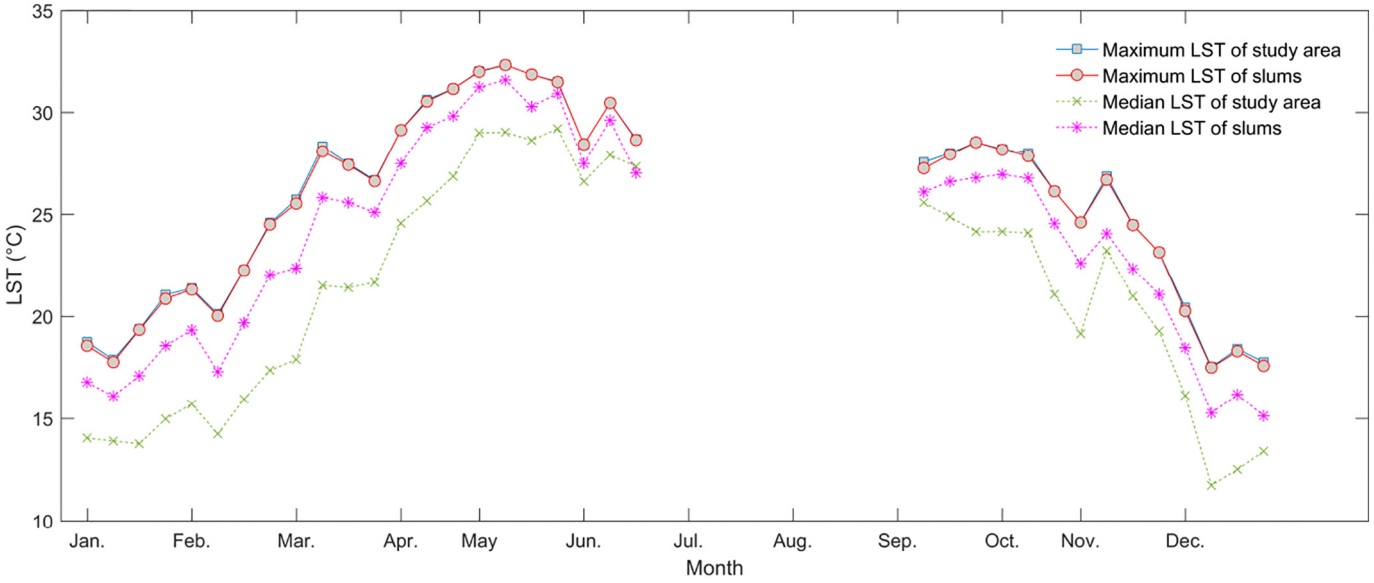

Fig. 10. The LST variations around slums through the entire year 2010 for the entire study area (missing data between late June and early September due to undesirable weather conditions).

Potential interpretations can be either that slum houses tend to be clustered at densely and poorly built locations producing locally high LST, or slums are also contributing to locally high LST. Beyond image-based approaches, census-based surveys and participatory mapping have already shown that slums are associated with specific site conditions including hazardous location and densely yet poorly built old city with job opportunities (Kohli et al., 2012). High building density, limited vegetation, and poor roof materials are also observed within slums (Davis, 2006; Kohli et al., 2012; Kuffer et al., 2017; Taubenböck and Kraff, 2014). The above conditions produce land surface specifications of high building density, limited sky view factor, low vegetation coverage, low surface albedo and high impervious surface coverage, which provoke high LST within and around slums (Wang and Ouyang, 2017). Quantifying relationships among the LST and the land surface specifications requires more detailed building level surveys or very high resolution 3-dimensional measurements, *e.g.* using Unmanned Aerial Vehicles (UAVs) (Gevaert et al., 2017; Gevaert et al., 2016; Sliuzas et al., 2017). Furthermore, the relationships at local scale can vary because the land surface specifications are combined and impact the LST differently across the city (Georgescu et al., 2014; Gill et al., 2007; Wang and Ouyang, 2017). For example, in Ahmedabad, slums in residential areas and industrial areas interact with local LST differently along with their surrounding environment. The relationship needs to be examined in more detail with surveys or high resolution data to identify how major land surface specifications impact local LST before prioritizing mitigation and adaptation strategies.

Finally, a preliminary year-round analysis is deployed to show how LST at places with slums varies through months compared to the study area (Fig. 10). All of the MODIS 8-day images at 01:30 in 2010 are used for year-round analysis resulting in 3 to 4 data points for each month. Only the maximum and median LSTs are shown. Due to the monsoon season between June and September, the LST data is substantially disturbed by frequent and abundant precipitation and thus no data can be shown. Similar to the information in Fig. 9, the maximum LST at places with slums is not necessarily yet very close to the highest LST of the study area throughout the year, whereas the median LST of places with slums is higher than that of the entire study area throughout the year.

5. Discussion

Examining the exposure of vulnerable slum dwellers to high temperature hazard is highly demanded, however, the temperature as a geographic phenomenon is dynamic and uncertain. Thus several theoretic, technical implications and limitations are worth discussing.

5.1. Using the LST as a proxy of near surface air temperature

Using LST patterns to investigate the heat exposure of slums brings the concern of how far one should proceed to use LST as a proxy of near surface air temperature variation. Due to the limited number of studies (Vancutsem et al., 2010; Zakšek and Schroedter-Homscheidt, 2009; Zhu et al., 2013), it is difficult to conclude that the correlation between LST and near surface air temperature is sufficiently understand (Tomlinson et al., 2011). Following the suggestion of using nighttime LST images with lower resolution to approximate the variation of near surface air temperature may, to a large extent, eliminate uncertainties (Kloog et al., 2014; Yan et al., 2009; Zhu et al., 2017), but it is strongly recommended to conduct a localized case-specific analysis of LST-air temperature coupling in future studies. In contrast, substantial parameterization is required to adjust the daytime LST to reach agreement with near surface air temperature (Voogt and Oke, 2003).

5.2. Characterizing the local scale heat patterns with enriched parameters

While vulnerability analysis has been extended into urban areas to focus on certain groups with lower socioeconomic levels, a localized analysis of exposure to hazard should also be conducted to localize risk evaluations. However, conventional heat related meteorological studies are commonly conducted at regional or city scale, ignoring the heat variations within urban areas. Recent local scale analysis of heat patterns within urban areas are locally aggregated or averaging temperature disregarding the fact that intrinsic temperature patterns are not restricted by the aggregation boundaries of neighborhoods, census tracts and land use patches(Coutts et al., 2016; Norton et al., 2015). The morphological-based characterization of LST patterns follows the suggestion of focusing on the intrinsic pattern of the meteorological phenomenon before relating it to any land surface factors (Oke, 1982).

The morphological features evaluated through the MSSI are not restricted by the pixel size or land use patches thus parameters derived from features properly capture the intrinsic patterns of the LST. Such an evaluation at the phenomenon level can be considered as a significant progress as previous studies focused on local temperature dynamics in artificially defined geographic units without considering the intrinsic variations and patterns of the phenomenon itself.

Parameters for characterizing local scale temperature patterns are highly demanded. Although the phenomenon of UHI has been documented for nearly 200 years (Howard, 1833), the characterization of the UHI by using geospatial techniques can be traced back for only the last 15 years marked by the milestone study of the UHI in Houston, US (Streutker, 2002). Spatial properties of the UHI (*e.g.*, the extent and range) have only been initiated recently along with the availability of geospatial data and advancement of modeling techniques. As the investigation reaches into local scale, existing parameters failed to delineate the spatial properties of the locally higher LST because of limitations in modeling techniques or data sources. Thus excessive heat is commonly investigated through solely comparing the temperature values. The morphological analysis adds to the spatial dimension complementing the current approach and providing the opportunity to understand more about dynamics and impacts of the high temperature especially for vulnerable groups at local scale. As the temperature value and the morphology of the temperature patterns capture different properties of the phenomenon, it is highly recommended to use parameters such as MSSI and curvedness along with existing ones such as diurnal temperature range (DTR), maximum, and minimum (Stewart, 2011a) to provide a full picture of temperature dynamics.

5.3. The dynamics of the LST

The LST as a geographic phenomenon is dynamic in both space and time. Biased conclusions are commonly drawn from limited observation of LST patterns at a certain scale and a particular point of time. Taking advantage of the high temporal resolution of MODIS data, this study has found that the LST in urban areas is higher during the nighttime and lower during the daytime compared to the rural surroundings, which can potentially be the opposite in other (less arid) cities. The findings are consistent with previous ones obtained in arid and non-arid cities (Charabi and Bakhit, 2011; Emmanuel and Fernando, 2007; Golden, 2004; Haashemi et al., 2016; Rasul et al., 2017; Tran et al., 2013; Wang et al., 2015a; Zhou et al., 2014). Thus defining places with high temperature should take this uncertainty into account. This leads to the uncertainty in the association between LST and land surface components. For instance, the locally high temperature at the places with slums can be substantially underestimated if only daytime LST is considered. Now, the findings in this study indicate that slums may suffer from the prolonged excessive heat during nighttime in addition to the daytime solar radiation.

5.4. Implications for sustainable and resilient urban development

The conventional three-pillar structure of environmental, social and economic sustainability has recently been redefined and shifted to a scheme where socioeconomic sustainability is encompassed by environmental sustainability (Wu, 2013). Understanding heat dynamics, human-climate interactions and environmental impacts of urban development form the foundation of sustainable socioeconomic development. In sustainable urban planning practice, decision makers and planners demand detailed guidelines that can be implemented stepwise and incrementally (Chang et al., 2007; Wang and Ouyang, 2017). Thus heat mitigation should be locally oriented. The localized analysis of the intrinsic patterns of the LST can bridge the gap between meteorology and urban planning. It provides the planning domain with the opportunity to prioritize and pinpoint localized mitigation targets (Stewart, 2011a).

Sustainable cities intrinsically rely on resilience to absorb, recover from and adapt to external disturbance (Marchese et al., 2018). Focusing on heat exposure of slums conforms to the rationale of improving urban resilience by starting with the most vulnerable groups exposed to hazards (Chu, 2015). Mitigation and adaptation of extreme heat within and around slums is equivalent to improving the lower bound of resilience of a city in coping with climate hazards. However, the dynamics of the LST addressed in Section 5.3 is also reflected in its formation mechanism. The dynamics hinder the identification of major land surface factors impacting the LST due to the time and location of observation, spatial heterogeneity and spatial diversity of land surface composition and configuration (Wang et al., 2016). This contributes to the frequently observed hesitation in establishing effective mitigation and adaptation policies (Georgescu et al., 2014; Gill et al., 2007). For instance, even though the increase of vegetation cover has been recognized as an efficient way to mitigate high temperature, planting vegetation in a place already covered by abundant trees with various types may bring distinctively different cooling consequences than in a place with a large fraction of impervious surface. This also applies to mitigating high LST at places with slums. Besides, the densely packed slum houses potentially signify the thermal effect of roofs, which require more detailed information through high resolution imagery or LiDAR point cloud in conjunction with micro-scale modeling to obtain the shape, orientation and albedo of the roofs (Ban-Weiss et al., 2015; Susca et al., 2011; Zhao et al., 2015). Thus effective mitigation strategies need to be developed after scrutinizing the relationship between the LST and land surface factors. Besides, land surface specification indicators are insufficiently recognized by decision makers and planners. While indicators such as vegetation coverage, impervious surface and building volumes can be modified through planning and design codes and regulations, other important heat responsive indicators such as sky view factors are yet be included into planning and design regulations. It means that increasing the transferability of knowledge in climate study to the planning domain is demanded for effective mitigation and adaptation policies.

6. Conclusions

Through exploring the exposure of slums to high temperature, this study develops a framework to examine the local scale morphological patterns of temperature. This morphological characterization facilitates the application of spatially sensitive parameters to the LST patterns and improves the understanding of the intrinsic pattern of the temperature phenomenon. The locally high temperature coincides with the presence of slums indicating that places with slums are exposed to an excessive heat compared to their local surroundings. Furthermore, the morphological parameters of the LST patterns indicate that larger slums are more likely to be located at places with a locally higher temperature. However, it is difficult to conclude if slums themselves partially govern the locally high temperature. By comparing the LST patterns at places with slums and those at places of other land use and cover types the study shows that places with slums are with higher temperature compared to places without slums. Due to the small size of slums, a sub-pixel level analysis is required for concluding whether slums contribute to the high temperature or whether slums are clustered at a poorly built environment already with high temperature.

There are two major implications of the study. Firstly, local scale investigation of the heat helps to better understand the potential hazard faced by vulnerable groups in urban areas, and progressively better captures the risks. Secondly, a local scale study of the temperature fills the research gap between meteorology and urban planning as planners and decision-makers are searching for more localized guidelines. Several issues need to be clarified and improved in future studies. For instance, the higher temporal resolution of MODIS data means detailed spatial variations of the LST are ignored and may lead to biased conclusions. In addition, the exposure to a heat hazard can be caused by not only

high temperature but also dramatic variation of temperature, thus temporal investigation of the temperature patterns is demanded.

Acknowledgments

The authors would like to acknowledge the support of the SimCity project (contract number: C.2324.0293) and Dynaslum (Data Driven Modelling and Decision Support for Slums) project (contract number: 27015G05), which are managed by the Dutch national research council (NWO) and the Dutch organization for ICT in education and research (SURF) to provide resources for this research.

Conflicts of interest

The authors declare no conflict of interest.

Appendix A

In mathematical formalization of the MTGP, the LST datasets D with the same spatial coverage and acquired at different times on different images can be defined as $D = \{(\mathbf{x}_i, t_{ij}) | i = 1,\ldots,n, j = 1,\ldots,m\}$, where $\mathbf{x}_i$ is the index of i^{th} spatial location in d dimensional space R^d (R^2 in this case), n is the number of pixels on one image, and m is the number of images considered as multi-tasks in the model ($m = 2$ in this case). Here, t_{ij} denotes the observed LST value at location $\mathbf{x}_i$ on the j^{th} image producing the multi-task formalization, where each task j corresponds to an image at a time containing n data points ($t_{1j},\ldots t_{nj}$). The MTGP imposes no exact prior form on the LST observations such as $t = f(\mathbf{x}) + \varepsilon$ with noise $\varepsilon \sim N(0, \sigma_n^2)$. Instead, it generalizes the function into an infinitely long vector $[f_1,\ldots,f_n]^T$. Any finite set of the vector is jointly Gaussian. The model $f(\mathbf{x}) \sim \mathrm{GP}(m(\mathbf{x}), K^f K^{\mathbf{x}})$ is completely specified by the mean function $m(\mathbf{x})$ and covariance function. K^f is a covariance structure incorporating the inter-task information shared between tasks, and $k^{\mathbf{x}}$ is the covariance between measurement locations. The Automatic Relevance Determinant (ARD) is applied as a 2-dimensional version of the Squared Exponential (SE) covariance function. Within the Bayesian scheme, make inference of latent LST value $\boldsymbol{f}^*$ becomes to solve the conditional probability and gives

$$\begin{aligned} P(\boldsymbol{f}^*|\mathbf{X}^*,\mathbf{X},\boldsymbol{t}) &= \int \left(P(\boldsymbol{f}^*|\mathbf{X},\boldsymbol{f}) \frac{P(\boldsymbol{t}|\mathbf{X},\boldsymbol{f})P(\boldsymbol{f}|\mathbf{X})}{\int P(\boldsymbol{t}|\mathbf{X},\boldsymbol{f})P(\boldsymbol{f}|\mathbf{X})d\boldsymbol{f}} \right) d\boldsymbol{f} \\ &\sim N\Big(\boldsymbol{M}(\boldsymbol{x}^*) + \boldsymbol{K}(\boldsymbol{x}^*,\boldsymbol{x})\left(\mathbf{K} + \sigma_n^2\mathbf{I}\right)^{-1}(\boldsymbol{t} - \boldsymbol{M}(\boldsymbol{x})) \Big), \\ &\quad \mathbf{K}(\boldsymbol{x}^*,\boldsymbol{x}^*) - \mathbf{K}(\boldsymbol{x}^*,\boldsymbol{x})\left[\mathbf{K}(\boldsymbol{x},\boldsymbol{x}) + \sigma_n^2\mathbf{I}\right]^{-1}\mathbf{K}(\boldsymbol{x},\boldsymbol{x}^*) \end{aligned} \quad . \tag{4}$$

The mean of the LST $\overline{\mathrm{f}^*}$ is achieved through

$$\overline{\mathrm{f}_j^*} = m(x^*) + \left(k^f \otimes k^x(x^*,x)\right)^T \left(K^f \otimes K^{\mathrm{x}} + \Delta \otimes I\right)^{-1}(\mathbf{t} - m(\mathbf{X})), \tag{5}$$

where $\otimes$ operates the Kronecker product of matrices or vectors. K^f and K^{x} are inter and intra-task covariance matrices, respectively. k^f is a column vector denoting task covariance involving inference. k^x is the covariance between locations, and Δ is a diagonal matrix in which noise σ^2 are recorded.

Machine learning is applied by using the normalizing term of the Bayesian structure in Eq. (4) to learn the hyper-parameters of the ARD covariance function, by maximizing the log marginal likelihood as

$$\begin{aligned} &\log \int P(\boldsymbol{t}|\mathbf{X},\boldsymbol{f})P(\boldsymbol{f}|\mathbf{X})d\boldsymbol{f} \\ &= -\frac{1}{2}\boldsymbol{t}\left(\mathbf{K} + \sigma_n^2\mathbf{I}\right)^{-1}\boldsymbol{t} - \frac{1}{2}\log|\mathbf{K} + \sigma_n^2\mathbf{I}| - \frac{n}{2}\log 2\pi. \end{aligned} \tag{6}$$

The trade-off between data fitting and model complexity is automatically controlled by the data fit term $-\boldsymbol{t}(\mathbf{K} + \sigma_n^2\mathbf{I})^{-1}\boldsymbol{t}$ and complexity penalty term $\log|\mathbf{K} + \sigma_n^2\mathbf{I}|$, which is referred as William of Occam's principle of "Plurality should not be assumed without necessity" (Rasmussen, 2006; Rasmussen and Ghahramani, 2001).

References

Amiri, R., Weng, Q., Alimohammadi, A., Alavipanah, S.K., 2009. Spatial–temporal dynamics of land surface temperature in relation to fractional vegetation cover and land use/cover in the Tabriz urban area, Iran. Remote Sens. Environ. 113, 2606–2617.
Anderson, J.R., 1976. A Land Use and Land Cover Classification System for Use With Remote Sensor Data. US Government Printing Office.
Arnfield, J., 2003. Two decades of urban climate research: a review of turbulence exchanges of energy and water, and the urban heat island. Int. J. Climatol. 23, 1–26.
Assembly, U.N.G., 2015. Sendai Framework for Disaster Risk Reduction 2015–2030 (In).
Azhar, G.S., Mavalankar, D., Nori-Sarma, A., Rajiva, A., Dutta, P., Jaiswal, A., Sheffield, P., Knowlton, K., Hess, J.J., 2014. Heat-related mortality in India: excess all-cause mortality associated with the 2010 Ahmedabad heat wave. PLoS One 9, e91831.
Baker, J.L., 2012. Climate Change, Disaster Risk, and the Urban Poor: Cities Building Resilience for a Changing World. World Bank, Washington, DC.
Balchin, W.G.V., Pye, N., 1947. A micro-climatological investigation of bath and the surrounding district. Q. J. R. Meteorol. Soc. 73, 297–323.
Ban-Weiss, G.A., Woods, J., Levinson, R., 2015. Using remote sensing to quantify albedo of roofs in seven California cities, part 1: methods. Sol. Energy 115, 777–790.
Blaikie, P., Cannon, T., Davis, I., Wisner, B., 2014. At Risk: Natural Hazards, People's Vulnerability and Disasters. Routledge.
Bonde, U., Badrinarayanan, V., Cipolla, R., 2013. Multi Scale Shape Index for 3d Object Recognition. Springer.
Bonilla, E., Chai, K.M., Williams, C., 2008. Multi-Task Gaussian Process Prediction.
Brooks, N., Adger, W.N., Kelly, P.M., 2005. The determinants of vulnerability and adaptive capacity at the national level and the implications for adaptation. Glob. Environ. Chang. 15, 151–163.
Buyantuyev, A., Wu, J., 2010. Urban heat islands and landscape heterogeneity: linking spatiotemporal variations in surface temperatures to land-cover and socioeconomic patterns. Landsc. Ecol. 25, 17–33.
Chandramouli, C., General, R., 2011. Census of India 2011. Provisional Population Totals. Government of India, New Delhi.
Chang, C.-R., Li, M.-H., Chang, S.-D., 2007. A preliminary study on the local cool-island intensity of Taipei city parks. Landsc. Urban Plan. 80, 386–395.
Change, I.P.o.C, 2014. Climate Change 2014–Impacts, Adaptation and Vulnerability: Regional Aspects. Cambridge University Press.
Charabi, Y., Bakhit, A., 2011. Assessment of the canopy urban heat island of a coastal arid tropical city: the case of Muscat, Oman. Atmos. Res. 101, 215–227.
Chaudhury, S., Gore, J., Ray, S., 2000. Heat wave impacts over India. Curr. Sci. 79, 153–155.
Chu, E., 2015. Urban Adaptations Observed: The Politics of Governing Climate Resilience in Indian Cities. Massachusetts Institute of Technology, In.
Connors, J.P., Galletti, C.S., Chow, W.T., 2013. Landscape configuration and urban heat island effects: assessing the relationship between landscape characteristics and land surface temperature in Phoenix, Arizona. Landsc. Ecol. 28, 271–283.
Coutts, A.M., Harris, R.J., Phan, T., Livesley, S.J., Williams, N.S., Tapper, N.J., 2016. Thermal infrared remote sensing of urban heat: hotspots, vegetation, and an assessment of techniques for use in urban planning. Remote Sens. Environ. 186, 637–651.
Dash, S., Kjellstrom, T., 2011. Workplace heat stress in the context of rising temperature in India. Curr. Sci. 496–503.
Davis, M., 2006. Planet of slums. N. Perspect. Q. 23, 6–11.
Emmanuel, R., Fernando, H., 2007. Urban heat islands in humid and arid climates: role of urban form and thermal properties in Colombo, Sri Lanka and Phoenix, USA. Clim. Res. 34, 241–251.
Garland, A.M., 2016. Innovation in urban development: incremental housing, Big Data and Gender. Wilson Center and USAID, Viewed January.
Georgescu, M., Morefield, P.E., Bierwagen, B.G., Weaver, C.P., 2014. Urban adaptation can roll back warming of emerging megapolitan regions. Proc. Natl. Acad. Sci. 111, 2909–2914.
Gevaert, C.M., Persello, C., Vosselman, G., 2016. Optimizing multiple kernel learning for the classification of UAV data. Remote Sens. 8, 1025.
Gevaert, C., Persello, C., Sliuzas, R., Vosselman, G., 2017. Informal settlement classification using point-cloud and image-based features from UAV data. ISPRS J. Photogramm. Remote Sens. 125, 225–236.
Gill, S.E., Handley, J.F., Ennos, A.R., Pauleit, S., 2007. Adapting cities for climate change: the role of the green infrastructure. Built Environ. (1978-) 115–133.
Golden, J.S., 2004. The built environment induced urban heat island effect in rapidly urbanizing arid regions–a sustainable urban engineering complexity. Environ. Sci. 1, 321–349.
Goodchild, M.F., 1987. A spatial analytical perspective on geographical information systems. Int. J. Geogr. Inf. Syst. 1, 327–334.
Göttsche, F.-M., Olesen, F.S., 2001. Modelling of diurnal cycles of brightness temperature extracted from METEOSAT data. Remote Sens. Environ. 76, 337–348.
Gulbe, L., Caune, V., Korats, G., 2017. Urban area thermal monitoring: Liepaja case study using satellite and aerial thermal data. Int. J. Appl. Earth Obs. Geoinf. 63, 45–54.
Haashemi, S., Weng, Q., Darvishi, A., Alavipanah, S.K., 2016. Seasonal variations of the surface urban heat island in a semi-arid city. Remote Sens. 8, 352.
Hajat, S., Armstrong, B.G., Gouveia, N., Wilkinson, P., 2005. Mortality displacement of heat-related deaths: a comparison of Delhi, Sao Paulo, and London. Epidemiology 16, 613–620.
Howard, L., 1818. The climate of London. W. Phillips, Sold Also by J. and A. Arch.

Howard, L., 1833. The Climate of London: Deduced From Meteorological Observations Made in the Metropolis and at Various Places Around It. Harvey and Darton, J. and A. Arch, Longman, Hatchard, S. Highley [and] R. Hunter.
Imhoff, M.L., Zhang, P., Wolfe, R.E., Bounoua, L., 2010. Remote sensing of the urban heat island effect across biomes in the continental USA. Remote Sens. Environ. 114, 504–513.
Kalnay, E., Cai, M., 2003. Impact of urbanization and land-use change on climate. Nature 423, 528–531.
Kjellstrom, T., Friel, S., Dixon, J., Corvalan, C., Rehfuess, E., Campbell-Lendrum, D., Gore, F., Bartram, J., 2007. Urban environmental health hazards and health equity. J. Urban Health 84, 86–97.
Klok, L., Zwart, S., Verhagen, H., Mauri, E., 2012. The surface heat island of Rotterdam and its relationship with urban surface characteristics. Resour. Conserv. Recycl. 64, 23–29.
Kloog, I., Nordio, F., Coull, B.A., Schwartz, J., 2014. Predicting spatiotemporal mean air temperature using MODIS satellite surface temperature measurements across the Northeastern USA. Remote Sens. Environ. 150, 132–139.
Knowlton, K., Kulkarni, S.P., Azhar, G.S., Mavalankar, D., Jaiswal, A., Connolly, M., Nori-Sarma, A., Rajiva, A., Dutta, P., Deol, B., 2014. Development and implementation of South Asia's first heat-health action plan in Ahmedabad (Gujarat, India). Int. J. Environ. Res. Public Health 11, 3473–3492.
Koenderink, J.J., van Doorn, A.J., 1992. Surface shape and curvature scales. Image Vis. Comput. 10, 557–564.
Kohli, D., Sliuzas, R., Kerle, N., Stein, A., 2012. An ontology of slums for image-based classification. Comput. Environ. Urban. Syst. 36, 154–163.
Kroeger, T., McDonald, R.I., Boucher, T., Zhang, P., Wang, L., 2018. Where the people are: current trends and future potential targeted investments in urban trees for PM 10 and temperature mitigation in 27 US cities. Landsc. Urban Plan. 177, 227–240.
Kuffer, M., Pfeffer, K., Sliuzas, R., Baud, I., Maarseveen, M.v., 2017. Capturing the diversity of deprived areas with image-based features: the case of Mumbai. Remote Sens. 9, 384.
Landsberg, H.E., 1981. The Urban Climate. Academic press.
Larsen, L., 2015. Urban climate and adaptation strategies. Front. Ecol. Environ. 13, 486–492.
Leal Filho, W., 2016. Innovation in Climate Change Adaptation. Springer.
Li, Z.-L., Tang, B.-H., Wu, H., Ren, H., Yan, G., Wan, Z., Trigo, I.F., Sobrino, J.A., 2013. Satellite-derived land surface temperature: current status and perspectives. Remote Sens. Environ. 131, 14–37.
Lowe, D.G., 1999. Object recognition from local scale-invariant features. Computer Vision, 1999. The Proceedings of the Seventh IEEE International Conference on. Ieee, pp. 1150–1157.
Marchese, D., Reynolds, E., Bates, M.E., Morgan, H., Clark, S.S., Linkov, I., 2018. Resilience and sustainability: similarities and differences in environmental management applications. Sci. Total Environ. 613, 1275–1283.
McGeehin, M.A., Mirabelli, M., 2001. The potential impacts of climate variability and change on temperature-related morbidity and mortality in the United States. Environ. Health Perspect. 109, 185.
Nag, P., Nag, A., Sekhar, P., Pandit, S., 2009. Vulnerability to Heat Stress: Scenario in Western India. 56. National Institute of Occupational Health, Ahmedabad.
Norton, B.A., Coutts, A.M., Livesley, S.J., Harris, R.J., Hunter, A.M., Williams, N.S.G., 2015. Planning for cooler cities: a framework to prioritise green infrastructure to mitigate high temperatures in urban landscapes. Landsc. Urban Plan. 134, 127–138.
Oke, T.R., 1973. City size and the urban heat island. Atmos. Environ. 7 (1967), 769–779.
Oke, T.R., 1981. Canyon geometry and the nocturnal urban heat island: comparison of scale model and field observations. J. Climatol. 1, 237–254.
Oke, T.R., 1982. The energetic basis of the urban heat island. Q. J. R. Meteorol. Soc. 108, 1–24.
Preston, B.L., Yuen, E.J., Westaway, R.M., 2011. Putting vulnerability to climate change on the map: a review of approaches, benefits, and risks. Sustain. Sci. 6, 177–202.
Quan, J., Chen, Y., Zhan, W., Wang, J., Voogt, J., Wang, M., 2014. Multi-temporal trajectory of the urban heat island centroid in Beijing, China based on a Gaussian volume model. Remote Sens. Environ. 149, 33–46.
Rajasekar, U., Weng, Q., 2009. Urban heat island monitoring and analysis using a non-parametric model: a case study of Indianapolis. ISPRS J. Photogramm. Remote Sens. 64, 86–96.
Rao, P., 1972. Remote sensing of urban heat islands from an environmental satellite. Am. Meteorol. Soc. 45 (In pp. 647-&: BEACON ST, BOSTON, MA 02108-3693).
Rasmussen, C.E., 2006. Gaussian Processes for Machine Learning.
Rasmussen, C.E., Ghahramani, Z., 2001. Occam's razor. Advances in Neural Information Processing Systems, pp. 294–300.
Rasul, A., Balzter, H., Smith, C., Remedios, J., Adamu, B., Sobrino, J.A., Srivanit, M., Weng, Q., 2017. A review on remote sensing of urban heat and cool islands. Land 6, 38.
Rathi, S., Desai, V., Jariwala, P., Desai, H., Naik, A., Joseph, A., 2017. Summer temperature and spatial variability of all-cause mortality in Surat city, India. Indian J. Community Med. 42, 111.
Romero-Lankao, P., Gnatz, D.M., Sperling, J.B., 2016. Examining urban inequality and vulnerability to enhance resilience: insights from Mumbai, India. Clim. Chang. 139, 351–365.
Roth, M., Oke, T., Emery, W., 1989. Satellite-derived urban heat islands from three coastal cities and the utilization of such data in urban climatology. Int. J. Remote Sens. 10, 1699–1720.
Sliuzas, R., Kuffer, M., Gevaert, C., Persello, C., Pfeffer, K., 2017. Slum mapping. Urban Remote Sensing Event (JURSE), 2017 Joint. IEEE, pp. 1–4.
Stewart, I.D., 2011a. Redefining the Urban Heat Island. University of British Columbia (Vancouver).
Stewart, I.D., 2011b. A systematic review and scientific critique of methodology in modern urban heat island literature. Int. J. Climatol. 31, 200–217.
Stewart, I., Oke, T., 2009. Newly developed "thermal climate zones" for defining and measuring urban heat island magnitude in the canopy layer. Eighth Symposium on Urban Environment. AZ, Phoenix.
Stewart, I.D., Oke, T.R., 2012. Local climate zones for urban temperature studies. Bull. Am. Meteorol. Soc. 93, 1879–1900.
Stocker, T., 2014. Climate Change 2013: The Physical Science Basis: Working Group I Contribution to the Fifth Assessment Report of the Intergovernmental Panel on Climate Change. Cambridge University Press.
Stoll, M.J., Brazel, A.J., 1992. Surface-air temperature relationships in the urban environment of Phoenix, Arizona. Phys. Geogr. 13, 160–179.
Stone, B., Vargo, J., Liu, P., Hu, Y., Russell, A., 2013. Climate change adaptation through urban heat management in Atlanta, Georgia. Environ. Sci. Technol. 47, 7780–7786.
Streutker, D.R., 2002. A remote sensing study of the urban heat island of Houston, Texas. Int. J. Remote Sens. 23, 2595–2608.
Streutker, D.R., 2003. Satellite-measured growth of the urban heat island of Houston, Texas. Remote Sens. Environ. 85, 282–289.
Susca, T., Gaffin, S.R., Dell'Osso, G., 2011. Positive effects of vegetation: urban heat island and green roofs. Environ. Pollut. 159, 2119–2126.
Svensson, M.K., Eliasson, I., 2002. Diurnal air temperatures in built-up areas in relation to urban planning. Landsc. Urban Plan. 61, 37–54.
Taubenböck, H., Kraff, N., 2014. The physical face of slums: a structural comparison of slums in Mumbai, India, based on remotely sensed data. J. Housing Built Environ. 29, 15–38.
Tomlinson, C.J., Chapman, L., Thornes, J.E., Baker, C., 2011. Remote sensing land surface temperature for meteorology and climatology: a review. Meteorol. Appl. 18, 296–306.
Tran, K.V., Azhar, G.S., Nair, R., Knowlton, K., Jaiswal, A., Sheffield, P., Mavalankar, D., Hess, J., 2013. A cross-sectional, randomized cluster sample survey of household vulnerability to extreme heat among slum dwellers in Ahmedabad, India. Int. J. Environ. Res. Public Health 10, 2515–2543.
Un-Habitat, 2016. Planning Sustainable Cities: Global Report on Human Settlements 2009. Routledge.
Vancutsem, C., Ceccato, P., Dinku, T., Connor, S.J., 2010. Evaluation of MODIS land surface temperature data to estimate air temperature in different ecosystems over Africa. Remote Sens. Environ. 114, 449–465.
Voogt, J.A., Oke, T.R., 1997. Complete urban surface temperatures. J. Appl. Meteorol. 36, 1117–1132.
Voogt, J.A., Oke, T.R., 2003. Thermal remote sensing of urban climates. Remote Sens. Environ. 86, 370–384.
Wan, Z., 2008. New refinements and validation of the MODIS land-surface temperature/emissivity products. Remote Sens. Environ. 112, 59–74.
Wan, Z., 2014. New refinements and validation of the collection-6 MODIS land-surface temperature/emissivity product. Remote Sens. Environ. 140, 36–45.
Wan, Z., Dozier, J., 1996. A generalized split-window algorithm for retrieving land-surface temperature from space. IEEE Trans. Geosci. Remote Sens. 34, 892–905.
Wang, J., Ouyang, W., 2017. Attenuating the surface Urban Heat Island within the Local Thermal Zones through land surface modification. J. Environ. Manag. 187, 239–252.
Wang, J., Huang, B., Fu, D., Atkinson, P.M., 2015a. Spatiotemporal variation in surface urban heat island intensity and associated determinants across major Chinese cities. Remote Sens. 7, 3670–3689.
Wang, J., Zhan, Q., Guo, H., 2015b. The morphology, dynamics and potential hotspots of land surface temperature at a local scale in urban areas. Remote Sens. 8, 18.
Wang, J., Qingming, Z., Guo, H., Jin, Z., 2016. Characterizing the spatial dynamics of land surface temperature–impervious surface fraction relationship. Int. J. Appl. Earth Obs. Geoinf. 45, 55–65.
Wigley, T.M., 2009. The effect of changing climate on the frequency of absolute extreme events. Clim. Chang. 97, 67–76.
Woodcock, C.E., Strahler, A.H., 1987. The factor of scale in remote sensing. Remote Sens. Environ. 21, 311–332.
Wu, J., 2013. Landscape sustainability science: ecosystem services and human well-being in changing landscapes. Landsc. Ecol. 28, 999–1023.
Yan, H., Zhang, J., Hou, Y., He, Y., 2009. Estimation of air temperature from MODIS data in East China. Int. J. Remote Sens. 30, 6261–6275.
Yin, C., Yuan, M., Lu, Y., Huang, Y., Liu, Y., 2018. Effects of urban form on the urban heat island effect based on spatial regression model. Sci. Total Environ. 634, 696–704.
Zakšek, K., Schroedter-Homscheidt, M., 2009. Parameterization of air temperature in high temporal and spatial resolution from a combination of the SEVIRI and MODIS instruments. ISPRS J. Photogramm. Remote Sens. 64, 414–421.
Zhao, Q., Myint, S., Wentz, E., Fan, C., 2015. Rooftop surface temperature analysis in an urban residential environment. Remote Sens. 7, 12135–12159.
Zhou, D., Zhao, S., Liu, S., Zhang, L., Zhu, C., 2014. Surface urban heat island in China's 32 major cities: spatial patterns and drivers. Remote Sens. Environ. 152, 51–61.
Zhu, W., Lű, A., Jia, S., 2013. Estimation of daily maximum and minimum air temperature using MODIS land surface temperature products. Remote Sens. Environ. 130, 62–73.
Zhu, W., Lű, A., Jia, S., Yan, J., Mahmood, R., 2017. Retrievals of all-weather daytime air temperature from MODIS products. Remote Sens. Environ. 189, 152–163.